Detection of turbulent thermal diffusion of particles in numerical simulations

Nils Erland L. Haugen, Nathan Kleeorin, Igor Rogachevskii, and Axel Brandenburg

Citation: Phys. Fluids **24**, 075106 (2012); doi: 10.1063/1.4733450
View online: http://dx.doi.org/10.1063/1.4733450
View Table of Contents: http://pof.aip.org/resource/1/PHFLE6/v24/i7
Published by the American Institute of Physics.

Detection of turbulent thermal diffusion of particles in numerical simulations

Nils Erland L. Haugen,[1,a)] Nathan Kleeorin,[2,b)] Igor Rogachevskii,[2,c)] and Axel Brandenburg[3,4,d)]
[1]*SINTEF Energy Research, N-7034 Trondheim, Norway*
[2]*Department of Mechanical Engineering, Ben-Gurion University of the Negev, P.O.Box 653, Beer-Sheva 84105, Israel*
[3]*NORDITA, Royal Institute of Technology and Stockholm University, Roslagstullsbacken 23, SE 10691 Stockholm, Sweden*
[4]*Department of Astronomy, Stockholm University, SE 10691 Stockholm, Sweden*

(Received 27 December 2011; accepted 19 June 2012; published online 12 July 2012)

The phenomenon of turbulent thermal diffusion in temperature-stratified turbulence causing a non-diffusive turbulent flux (i.e., non-counter-gradient transport) of inertial and non-inertial particles in the direction of the turbulent heat flux is found using direct numerical simulations (DNS). In simulations with and without gravity, this phenomenon is found to cause a peak in the particle number density around the minimum of the mean fluid temperature for Stokes numbers less than 1, where the Stokes number is the ratio of particle Stokes time to turbulent Kolmogorov time at the viscous scale. Turbulent thermal diffusion causes the formation of inhomogeneities in the spatial distribution of inertial particles whose scale is large in comparison with the integral scale of the turbulence. The strength of this effect is maximum for Stokes numbers around unity, and decreases again for larger values. The dynamics of inertial particles is studied using Lagrangian modelling in forced temperature-stratified turbulence, whereas non-inertial particles and the fluid are described using DNS in an Eulerian framework. [http://dx.doi.org/10.1063/1.4733450]

I. INTRODUCTION

Transport and mixing of small particles (aerosols and droplets) in turbulent fluid flow is of fundamental importance in a large variety of applications (environmental sciences, physics of the atmosphere and meteorology, industrial turbulent flows and turbulent combustion).[1–9] There are also astrophysical applications, in particular in the context of protoplanetary accretion discs.[10–13]

Numerous laboratory[4,14–18] and numerical[19–25] experiments as well as observations in atmospheric[7,9,26,27] and astrophysical[10–13,28,29] turbulent flows have shown different kinds of large-scale and small-scale long-living inhomogeneities (clusters) in the spatial distribution of particles. It is well known that turbulent diffusion causes the destruction of inhomogeneities in the spatial distributions of particles when the scale of the inhomogeneities is larger than the turbulent integral scale. But how can we explain the opposite process resulting in the formation of clusters of particles at scales larger than the integral scale?

One of the mechanisms of formation of particle inhomogeneities in temperature-stratified turbulence is the phenomenon of turbulent *thermal* diffusion.[30,31] This effect consists of a turbulent non-diffusive flux of inertial particles in the direction of the turbulent heat flux, so that particles

a)Nils.E.Haugen@sintef.no.
b)nat@bgu.ac.il.
c)gary@bgu.ac.il. URL: www.bgu.ac.il/∼gary.
d)brandenb@nordita.org. URL: www.nordita.org/∼brandenb.

are accumulated in the vicinity of the mean temperature minimum. The particular form of the flow field does not play any role in this effect. It is a purely collective phenomenon caused by temperature-stratified turbulence resulting in a pumping effect, i.e., the appearance of a non-zero mean effective velocity of particles in the direction opposite to the mean temperature gradient. A competition between two different phenomena, namely, the turbulent thermal diffusion and ordinary turbulent diffusion determines the conditions for the formation of large-scale particle clusters in the vicinity of the mean temperature minimum. The characteristic scale of the particle inhomogeneity formed due to turbulent thermal diffusion is much larger than the integral scale of the turbulence. Furthermore, the characteristic time scale of the formation of the particle inhomogeneity is much longer than the characteristic turbulent time, i.e., this is a mean-field effect.

Diffusive flux implies an effect that is determined by the second spatial derivative in the equation for the particle number density. This is the standard diffusion term that determines the counter-gradient transport in the particle flux. On the other hand, the non-diffusive flux implies a non-gradient transport in the particle flux. It is determined, e.g., by the first spatial derivative in the equation for the particle number density.

The phenomenon of turbulent thermal diffusion has been predicted theoretically[30,31] and detected in different laboratory experiments in stably and unstably temperature-stratified turbulence produced by oscillating grids or a multi-fan generator.[32–36] This phenomenon is shown to be important for atmospheric turbulence with temperature inversions[37] and for small-scale particle clustering in temperature-stratified turbulence,[36] but it is also expected to be significant for different kinds of heat exchangers, e.g., industrial boilers where Reynolds numbers and temperature gradients are large.

In spite of the fact that turbulent thermal diffusion has already been found in different types of laboratory experiments and atmospheric flows, this effect has never been studied in direct numerical simulations. The main goal of this paper is to find turbulent thermal diffusion of non-inertial and inertial particles in direct numerical simulations (DNS).

The paper is organized as follows. In Sec. II we discuss the physics of the phenomenon of turbulent thermal diffusion. The numerical simulations for fluid, inertial and non-inertial particles, and the results of direct numerical simulations are described in Sec. III. Motions of inertial particles are determined using a Lagrangian framework (Secs. III B–III D), while non-inertial particles are described using an Eulerian framework (Sec. III E). Discussion and conclusions are drawn in Sec. IV.

II. PHYSICS OF TURBULENT THERMAL DIFFUSION

In this section we discuss the physics of the phenomenon of turbulent thermal diffusion. The number density $n_p(t, \boldsymbol{r})$ of particles advected in a turbulent flow is determined by the following classical advection-diffusion equation:[38,39]

$$\frac{\partial n_p}{\partial t} + \boldsymbol{\nabla}\cdot(n_p \boldsymbol{U}_{\rm p} - D\boldsymbol{\nabla} n_p) = 0, \tag{1}$$

where D is the coefficient of Brownian diffusion of particles and $\boldsymbol{U}_{\rm p}$ is the particle velocity, which they acquire in a turbulent fluid velocity field $\boldsymbol{U}$. To study the formation of large-scale inhomogeneous particle structures, Eq. (1) for the particle number density is averaged over an ensemble of turbulent velocity fields. Using a mean-field approach, we decompose the particle number density n_p into the mean number density, $N = \overline{n_p}$ and fluctuations n, where $\overline{n} = 0$. We decompose the velocity field in a similar fashion. We assume for simplicity vanishing mean particle velocity, $\overline{\boldsymbol{U}_{\rm p}} = 0$. Averaging Eq. (1) over an ensemble of turbulent velocity fields we obtain an equation for the mean number density of particles,

$$\frac{\partial N}{\partial t} + \boldsymbol{\nabla}\cdot\left[\overline{n\,\boldsymbol{U}_{\rm p}} - D\,\boldsymbol{\nabla} N\right] = 0\,, \tag{2}$$

where $\overline{n\,\boldsymbol{U}_{\rm p}}$ is the turbulent flux of particles. To obtain a closed mean-field equation one needs to determine the turbulent flux of particles.

Already simple arguments[40] yield an estimate for the turbulent flux of particles $\overline{n\,\boldsymbol{U}_{\rm p}}$. Subtracting the averaged Eq. (2) from Eq. (1) we obtain an equation for the fluctuations of the particle number density, $n = n_p - N$,

$$\frac{\partial n}{\partial t} + \boldsymbol{\nabla}\cdot\left[n\,\boldsymbol{U}_{\rm p} - \overline{n\,\boldsymbol{U}_{\rm p}} - D\boldsymbol{\nabla} n\right] = -\boldsymbol{\nabla}\cdot(N\,\boldsymbol{U}_{\rm p}). \tag{3}$$

The left hand side of Eq. (3) has the dimension n/τ, where the time τ can be identified with the fluid turbulent integral timescale $\tau_{\rm f}$ for large fluid Reynolds numbers. (The subscript f stands for forcing scale.) Replacing the left hand side of Eq. (3) by $n/\tau_{\rm f}$ we obtain the following estimate for the fluctuations of the particle number density:

$$n \sim -\tau_{\rm f}\,(\boldsymbol{\nabla}\cdot\boldsymbol{U}_{\rm p})\,N - \tau_{\rm f}\,(\boldsymbol{U}_{\rm p}\cdot\boldsymbol{\nabla})N. \tag{4}$$

Multiply Eq. (4) by $\boldsymbol{U}_{\rm p}$ and average over an ensemble of turbulent velocity fields, we arrive at a formula for the turbulent flux of particles,

$$\overline{n\,\boldsymbol{U}_{\rm p}} = N\,\boldsymbol{V}^{\rm eff} - \boldsymbol{D}_T\,\boldsymbol{\nabla} N, \tag{5}$$

where the first term on the right hand side of Eq. (5), $N\,\boldsymbol{V}^{\rm eff}$, describes the turbulent flux of particles due to turbulent thermal diffusion, and the effective velocity is

$$\boldsymbol{V}^{\rm eff} = -\tau_{\rm f}\,\overline{\boldsymbol{U}_{\rm p}\,(\boldsymbol{\nabla}\cdot\boldsymbol{U}_{\rm p})}. \tag{6}$$

The second term on the right hand side of Eq. (5), $-\boldsymbol{D}_T\,\boldsymbol{\nabla} N$, determines the flux of particles caused by turbulent diffusion,

$$\boldsymbol{D}_T\,\boldsymbol{\nabla} N = \tau_{\rm f}\,\overline{(\boldsymbol{U}_{\rm p})_i\,(\boldsymbol{U}_{\rm p})_j}\,\nabla_j N \approx \tau_{\rm f}\,\overline{U_i\,U_j}\,\nabla_j N, \tag{7}$$

where $\boldsymbol{D}_T = \tau_{\rm f}\,\overline{U_i\,U_j}$ is the turbulent diffusion tensor and we have assumed here that the Stokes number is small, so that $\boldsymbol{U}_{\rm p} \sim \boldsymbol{U}$. For instance, for isotropic turbulence we have $\boldsymbol{D}_T = D_T\delta_{ij}$, where $D_T = \tau_{\rm f}\,\overline{\boldsymbol{U}^2}/3$. The turbulent flux of particles determined by Eqs. (5)–(7), coincides with that derived using rigorous approaches.[30,31,37,41–44]

A. Non-inertial particles

Let us first consider non-inertial particles advected by the fluid flow such that the particle velocity coincides with the fluid velocity, $\boldsymbol{U}_{\rm p} = \boldsymbol{U}$. The equation for the mean number density, N, of the non-inertial particles is

$$\frac{\partial N}{\partial t} + \boldsymbol{\nabla}\cdot\left[N\,\boldsymbol{V}^{\rm eff} - (D + D_{\rm T})\,\boldsymbol{\nabla} N\right] = 0; \tag{8}$$

see Eqs. (2) and (5)–(7). For low Mach numbers, using the anelastic approximation, $\boldsymbol{\nabla}\cdot\boldsymbol{U} \approx -\boldsymbol{U}\cdot\boldsymbol{\nabla}\ln\rho$, the effective velocity of non-inertial particles is given by

$$V_i^{\rm eff} = -\tau_{\rm f}\,\overline{U_i\,(\boldsymbol{\nabla}\cdot\boldsymbol{U})} = \tau_{\rm f}\,\overline{U_i\,U_j}\,\nabla_j\,\ln\overline{\rho}, \tag{9}$$

where $\overline{\rho}$ is the mean fluid density. When $\boldsymbol{\nabla}\,\overline{p} = \boldsymbol{0}$ and the anisotropy of the turbulence is weak, the effective velocity of non-inertial particles is,

$$\boldsymbol{V}^{\rm eff} = D_{\rm T}\,\boldsymbol{\nabla}\,\ln\overline{\rho} = -D_{\rm T}\,\boldsymbol{\nabla}\ln\overline{T}, \tag{10}$$

where $\overline{p}$ is the mean fluid pressure and $\overline{T}$ is the mean fluid temperature. The steady-state solution of Eqs. (8) and (10) for the mean number density of non-inertial particles is given by

$$\tilde{N}(z) = [\tilde{\rho}(z)]^{\frac{D_{\rm T}}{D+D_{\rm T}}}, \tag{11}$$

where $\tilde{N} = N/N_0$ is the non-dimensional mean number density of particles, $\tilde{\rho}(z) = \overline{\rho}/\overline{\rho}_0$ is the non-dimensional mean fluid density, and the subscripts 0 represent the values far from the cooling zone. Equation (11) implies that small particles are accumulated in the vicinity of the maximum of the fluid density.

TABLE I. Mechanism of particle transport $\overline{n\,\boldsymbol{U}}$ for non-inertial particles along the direction of the mean fluid density gradient.

$\longrightarrow \nabla\overline{\rho}$	
a	b
$U_x > 0$	$U_x < 0$
$\boldsymbol{\nabla}\cdot\boldsymbol{U} < 0$	$\boldsymbol{\nabla}\cdot\boldsymbol{U} > 0$
$n > 0$	$n < 0$
$n\,U_x > 0$	$n\,U_x > 0$
$\longrightarrow \overline{n\,\boldsymbol{U}}$	

Indeed, the non-diffusive flux of particles, $N\,\boldsymbol{V}^{\rm eff}$, is directed toward the maximum of the fluid density [see Eq. (10)]. The physics of the accumulation of non-inertial particles in the vicinity of the maximum of the mean fluid density (or the minimum of the mean fluid temperature) can be explained as follows (see Table I). Let us assume that the mean fluid density $\overline{\rho}_2$ at point 2 is larger than the mean fluid density $\overline{\rho}_1$ at point 1. Consider two small control volumes "a" and "b" located between these two points, and let the direction of the local turbulent velocity in volume "a" at some instant be the same as the direction of the mean fluid density gradient $\boldsymbol{\nabla}\,\overline{\rho}$ (i.e., along the x axis toward point 2). Let the local turbulent velocity in volume "b" at this instant be directed opposite to the mean fluid density gradient (i.e., toward point 1).

In a fluid flow with an imposed mean temperature gradient (i.e., an imposed mean fluid density gradient), one of the sources of particle number density fluctuations, $n \propto -\tau_{\rm f}\,N\,(\boldsymbol{\nabla}\cdot\boldsymbol{U})$, is caused by a non-zero $\boldsymbol{\nabla}\cdot\boldsymbol{U} \approx -\boldsymbol{U}\cdot\boldsymbol{\nabla}\ln\rho \neq 0$ [see the first term on the right hand side of Eq. (4)]. Since fluctuations of the fluid velocity $\boldsymbol{U}$ are positive in volume "a" and negative in volume "b," we have $\boldsymbol{\nabla}\cdot\boldsymbol{U} < 0$ in volume "a," and $\boldsymbol{\nabla}\cdot\boldsymbol{U} > 0$ in volume "b." Therefore, the fluctuations of the particle number density $n \propto -\tau_{\rm f}\,N\,(\boldsymbol{\nabla}\cdot\boldsymbol{U})$ are positive in volume "a" and negative in volume "b." However, the flux of particles $n\,U_x$ is positive in volume "a" (i.e., it is directed toward point 2), and it is also positive in volume "b" (because both fluctuations of fluid velocity and number density of particles are negative in volume "b"). Therefore, the mean flux of particles $\overline{n\,\boldsymbol{U}}$ is directed, as is the mean fluid density gradient $\boldsymbol{\nabla}\,\overline{\rho}$, toward point 2. This forms large-scale heterogeneous structures of non-inertial particles in regions with a mean fluid density maximum.

B. Inertial particles

Let us now discuss the transport of inertial particles. The non-diffusive mean flux of particles, $N\,\boldsymbol{V}^{\rm eff}$, toward the mean temperature minimum is the main reason for the formation of large-scale inhomogeneous distributions of inertial particles in temperature-stratified turbulence. Indeed, an equation for the mean number density, N, of inertial particles is given by

$$\frac{\partial N}{\partial t} + \boldsymbol{\nabla}\cdot\left[N\,(\boldsymbol{W}_{\rm g} + \boldsymbol{V}^{\rm eff}) - (D + D_{\rm T})\,\boldsymbol{\nabla}N\right] = 0\,, \tag{12}$$

where for inertial particles we have taken into account the effect of gravity, i.e., $\boldsymbol{W}_{\rm g} = \tau_{\rm p}\,\boldsymbol{g}$ is the terminal fall velocity of particles, $\boldsymbol{g}$ is the gravitational acceleration, and

$$\boldsymbol{V}^{\rm eff} = -\tau_{\rm f}\,\overline{\boldsymbol{U}_{\rm p}\,(\boldsymbol{\nabla}\cdot\boldsymbol{U}_{\rm p})} = -\alpha\,D_{\rm T}\,\boldsymbol{\nabla}\ln\overline{T} \tag{13}$$

is the effective pumping velocity of particles due to turbulent thermal diffusion. For large Péclet numbers the coefficient α is unity for non-inertial particles, while for inertial particles α depends on $\tau_{\rm p}$, the Mach number and the fluid Reynolds number,[30,31,37] where $\tau_{\rm p}$ is the Stokes time that describes particle-fluid interactions. The steady-state solution of Eqs. (12) and (13) for the mean number density of inertial particles is given by

$$\tilde{N}(z) = [\tilde{T}(z)]^{-\frac{\alpha D_{\rm T}}{D+D_{\rm T}}}\,\exp\left[-\int_{z_0}^{z}\frac{W_{\rm g}}{D + D_{\rm T}}\,{\rm d}z'\right], \tag{14}$$

TABLE II. Mechanism of particle transport $\overline{n\,\boldsymbol{U}_p}$ for inertial particles along the direction of turbulent heat flux.

	$\longrightarrow \overline{\boldsymbol{U}\theta}$	
a		b
$U_{px} > 0$		$U_{px} < 0$
$\theta > 0$		$\theta < 0$
$p > 0$		$p < 0$
$\boldsymbol{\nabla}\cdot\boldsymbol{U}_\mathrm{p} < 0$		$\boldsymbol{\nabla}\cdot\boldsymbol{U}_\mathrm{p} > 0$
$n > 0$		$n < 0$
$n\,U_{px} > 0$		$n\,U_{px} > 0$
	$\longrightarrow \overline{n\,\boldsymbol{U}_\mathrm{p}}$	

where $W_\mathrm{g} = |\boldsymbol{W}_\mathrm{g}|$ is the modulus of the terminal fall velocity, $\tilde{T} = \overline{T}/\overline{T}_0$ is the non-dimensional mean fluid temperature, and the subscripts 0 represent the values far from the cooling zone. Equation (14) implies that small particles are accumulated in the vicinity of the mean temperature minimum.

In the following we explain the mechanism[30,31] of turbulent thermal diffusion for inertial particles with material density ρ_p being much larger than the fluid density ρ. The inertia causes particles inside the turbulent eddies to drift out to the boundary regions between eddies. This can be seen by considering the equation of motion for particles, $\mathrm{d}\boldsymbol{U}_\mathrm{p}/\mathrm{d}t = -(\boldsymbol{U}_\mathrm{p} - \boldsymbol{U})/\tau_\mathrm{p}$, where, for simplicity, the gravity force is neglected. The solution of the equation of motion for small Stokes time reads[45]

$$\boldsymbol{U}_\mathrm{p} = \boldsymbol{U} - \tau_\mathrm{p}\,\frac{\mathrm{d}\boldsymbol{U}}{\mathrm{d}t} + \mathrm{O}(\tau_\mathrm{p}^2). \tag{15}$$

For large Reynolds numbers, this yields,

$$\boldsymbol{\nabla}\cdot\boldsymbol{U}_\mathrm{p} = \boldsymbol{\nabla}\cdot\boldsymbol{U} + \frac{\tau_\mathrm{p}}{\rho}\,\boldsymbol{\nabla}^2 p + \mathrm{O}(\tau_\mathrm{p}^2), \tag{16}$$

where p is the fluid pressure. For large Péclet numbers, when molecular diffusion of particles in Eq. (1) can be neglected, it follows that $\boldsymbol{\nabla}\cdot\boldsymbol{U}_\mathrm{p} \propto -\mathrm{d}\ln n_p/\mathrm{d}t$. Therefore, in regions with maximum fluid pressure (i.e., where $\boldsymbol{\nabla}^2 p < 0$), there is accumulation of inertial particles, i.e., $\mathrm{d}n_p/\mathrm{d}t \propto -N\,(\tau_\mathrm{p}/\overline{\rho})\,\boldsymbol{\nabla}^2 p > 0$. These regions have low vorticity, high strain rate, and maximum fluid pressure. Similarly, there is an outflow of inertial particles from regions with minimum fluid pressure.

In homogeneous and isotropic turbulence without mean gradients of temperature, a drift from regions with increased concentration of particles by a turbulent flow is equiprobable in all directions, and the pressure (temperature) of the surrounding fluid is not correlated with the turbulent velocity field. The only non-zero correlation is $\overline{(\boldsymbol{U}\cdot\boldsymbol{\nabla})p}$ which contributes to the energy flux, while $\overline{\boldsymbol{U}\,p} = 0$.

In temperature-stratified turbulence, temperature and velocity fluctuations are correlated due to a non-zero turbulent heat flux, $\overline{\boldsymbol{U}\,\theta} \neq \boldsymbol{0}$, where θ is the fluid temperature fluctuation. Fluctuations of temperature cause pressure fluctuations, which result in fluctuations of the number density of particles.

Increase of the pressure of the surrounding fluid is accompanied by an accumulation of particles, and the direction of the mean flux of particles coincides with that of the turbulent heat flux. The mean flux of particles is directed toward the minimum of the mean temperature, and the particles tend to be accumulated in this region.[30,37,41,42] To demonstrate that the directions of the mean flux of particles and the turbulent heat flux coincide, we assume that the mean temperature T_2 at point 2 is larger than the mean temperature T_1 at point 1 in Table II. We consider two small control volumes "a" and "b" located between these two points; see Table II. Let the direction of the local turbulent velocity in volume "a" at some instant be control volume "a" at some instant be the same as the direction of the turbulent heat flux $\overline{\boldsymbol{U}\,\theta}$ (i.e., along the x axis toward point 1) and let the local turbulent velocity in volume "b," at the same instant, be directed opposite to the turbulent heat flux (i.e., toward point 2).

In temperature-stratified turbulence with a non-zero turbulent heat flux $\overline{\boldsymbol{U}\,\theta}$, fluctuations of pressure p and velocity $\boldsymbol{U}$ are correlated, and regions with a higher level of pressure fluctuations have higher temperature and velocity fluctuations.[46,47] The fluctuations of temperature θ and pressure p in volume "a" are positive because $U_x\,\theta > 0$, and negative in volume "b"; see Table II. The fluctuations of particle number density n are positive in volume "a" (because particles are locally accumulated in the vicinity of the maximum of pressure fluctuations, $\mathrm{d}n/\mathrm{d}t \propto -N\,(\tau_\mathrm{p}/\overline{\rho})\,\boldsymbol{\nabla}^2 p > 0$), and they are negative in volume "b" (because there is an outflow of particles from regions with low pressure). The flux of particles $n\,U_\mathrm{px}$ is positive in volume "a" (i.e., it is directed toward point 1), and it is also positive in volume "b" (because both fluctuations of velocity and number density of particles are negative in volume "b"), where U_px is the particle velocity along the x axis. Therefore, the mean flux of particles $\overline{n\,\boldsymbol{U}_p}$ is directed, as is the turbulent heat flux $\overline{\boldsymbol{U}\,\theta}$, toward point 1. This causes the formation of large-scale inhomogeneous structures in the spatial distribution of inertial particles in the vicinity of the mean temperature minimum.

Note that turbulent thermal diffusion and turbulent diffusion are two principally different phenomena. Turbulent diffusion is described by second-order spatial derivatives, while turbulent thermal diffusion is determined by first-order spatial derivatives in the equation for the mean particle number density. In that sense turbulent thermal diffusion is a non-diffusive effect. Molecular thermal diffusion of gases (also called the Soret effect) or thermophoresis of particles are also non-diffusive effects because they are determined by first-order spatial derivatives. However, the mechanism of turbulent thermal diffusion is principally different from molecular thermophoresis and molecular thermal diffusion. Indeed, the phenomenon of turbulent thermal diffusion of inertial particles occurs due to the combined action of turbulence effects and particle inertia effects, while molecular thermophoresis is caused by purely kinetic effects related to the thermal motion of molecules. In a stratified turbulent flow turbulent thermal diffusion and molecular thermophoresis occur simultaneously, although the effect of turbulent thermal diffusion for large Reynolds and Peclet numbers is essentially stronger than the effect of molecular thermophoresis. In particular, the ratio of effective velocity due to turbulent thermal diffusion and velocity caused by molecular thermophoresis is of the order of the Reynolds number.[37] In this estimate we have used the formula for the molecular thermophoretic velocity,[48] $V_\mathrm{th} \sim \nu\,|\boldsymbol{\nabla} T|/T$, and the formula for the effective velocity caused by turbulent thermal diffusion.

In addition, there is also turbophoresis. This mean-field effect is related to particle inertia in systems with non-uniform turbulence intensity causing an additional mean particle velocity.[49,50] The turbophoresis and turbulent thermal diffusion are distinct phenomena. The effective particle velocity due to the phenomenon of turbulent thermal diffusion originates from the turbulent particle flux, i.e., it describes a collective statistical phenomenon, while the mean particle velocity due to turbophoresis originates directly from the expression for mean particle velocity.

III. DIRECT NUMERICAL SIMULATIONS

A. DNS model for the fluid

In this study, equations for the fluid are solved by employing DNS in an Eulerian framework. All numerical simulations have been performed using the PENCIL CODE[51] (for details of the code, see Refs. 29 and 52). The set of compressible hydrodynamic equations is solved for the fluid density ρ, the fluid velocity $\boldsymbol{U}$, and the specific entropy s,

$$\frac{\mathrm{D}\ln\rho}{\mathrm{D}t} = -\boldsymbol{\nabla}\cdot\boldsymbol{U}, \tag{17}$$

$$\frac{\mathrm{D}\boldsymbol{U}}{\mathrm{D}t} = -\frac{1}{\rho}\left[\boldsymbol{\nabla} p - \boldsymbol{\nabla}\cdot(2\rho\nu\mathbf{S})\right] + \boldsymbol{f}, \tag{18}$$

$$T\frac{\mathrm{D}s}{\mathrm{D}t} = \frac{1}{\rho}\boldsymbol{\nabla}\cdot K\boldsymbol{\nabla} T + 2\nu\mathbf{S}^2 - c_\mathrm{P}(T - T_\mathrm{ref}), \tag{19}$$

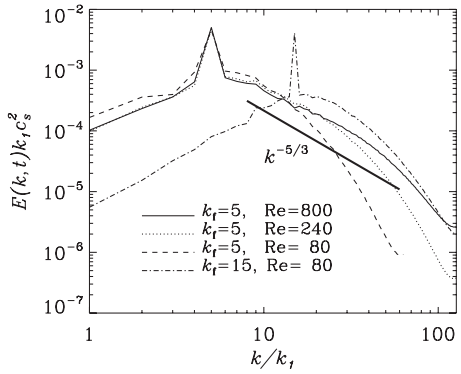

FIG. 1. The velocity power spectrum is shown for the simulation with forcing at $k_f = 15$ together with three simulations with forcing at $k_f = 5$ but for different Reynolds numbers.

where $T = T_0 \exp(s/c_V)(\rho/\rho_0)^{\gamma-1}$ is the fluid temperature, $\gamma = c_P/c_V$ is the ratio of specific heats at constant pressure and volume, respectively, $\mathrm{D}/\mathrm{D}t = \partial/\partial t + \boldsymbol{U}\cdot\boldsymbol{\nabla}$ is the advective derivative, $\boldsymbol{f}$ is the external forcing function, $p = (c_P - c_V)\rho T$ is the fluid pressure, ν is the kinematic viscosity, and K is the thermal conductivity. The traceless rate of strain tensor is given by

$$\mathsf{S}_{ij} = \frac{1}{2}(U_{i,j} + U_{j,i}) - \frac{1}{3}\delta_{ij}\boldsymbol{\nabla}\cdot\boldsymbol{U},$$

where $U_{i,j} = \nabla_j U_i$. The last term in the entropy Eq. (19) determines the cooling, which causes a temperature minimum at $z = 0$, where

$$T_{\mathrm{ref}} = T_0 - \delta T \ \exp(-z^2/2\sigma^2),$$

and z is the vertical coordinate. Therefore, the temperature minimum is located at the center of the box. Above the mean temperature minimum the turbulence is stably stratified, while below the mean temperature minimum the turbulence is unstably stratified.

The size of the simulation domain is L in all three directions. The smallest wavenumber in the domain, $k_1 = 2\pi/L$. Wavenumbers are measured in units of k_1, and lengths in units of k_1^{-1}. The width of the cooling function is $\sigma = 0.5/k_1$. Furthermore, the strength of the cooling function, δT, is such that the relative contrast between temperature maximum and temperature minimum is $\sim$1.6. In all simulations the Prandtl number $\mathrm{Pr} = \nu/\chi = 1$, where $\chi = K/\rho c_P$ is the temperature diffusivity.

Turbulence in the simulation box is produced by the forcing function $\boldsymbol{f}$, which is solenoidal and non-helical, i.e., $\boldsymbol{\nabla}\cdot\boldsymbol{f} = \boldsymbol{f}\cdot\boldsymbol{\nabla}\times\boldsymbol{f} = 0$, and injects energy and momentum perpendicular to a random wavevector whose direction changes every timestep, but its length is $\sim k_{\mathrm{f}}$ (see Ref. 53). The strength of the forcing is set such that the maximum Mach number is below 0.5.

In Fig. 1, velocity power spectra are shown for different simulations such that $\int E(k,t)dk = u_{\mathrm{rms}}^2$. It can be seen that for the simulations with $k_f = 5$ and $\mathrm{Re} \geq 240$ some inertial range scaling is present. For the simulation with $\mathrm{Re} = 800$ even some parts of the bottleneck can be seen.[54] In Fig. 2 the instantaneous velocity field is shown for the simulation with forcing at $k_f = 15$ and $\mathrm{Re} = 800$. In Fig. 3 u_{rms} is shown as a function of vertical position for the three spatial dimensions. The rms velocity is calculated as follows (showing $u_{\mathrm{rms}}(x)$ as an example); $u_{\mathrm{rms}}(x) = \sum_{j,k}\boldsymbol{U}(x, y_j, z_k)^2/N_{j,k}$, where y_j and z_k are the y and z coordinates for grid point number j and k, respectively. $N_{j,k} = j_{\max}k_{\max}$ is the total number of grid points in a given x plane.

B. Lagrangian model for inertial particles

The equation of motion of the inertial particles is solved numerically in a Lagrangian framework. Particles are treated as point particles and we consider the one-way coupling approximation, i.e., there is an effect of the fluid on the particles only, while the particles do not influence the fluid motions. This is a good approximation when the spatial density of particles is much smaller than the

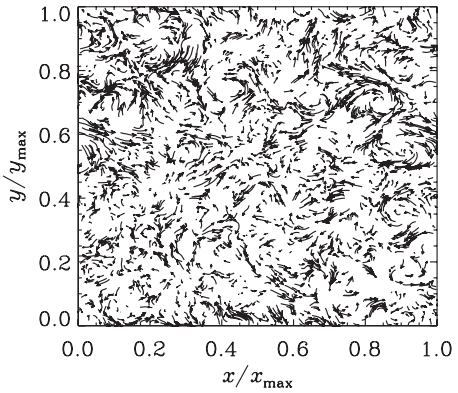

FIG. 2. The instantaneous velocity field in the *xy* plane for a simulation with forcing at $k_f = 15$ and $\mathrm{Re} = 800$.

fluid density. The particle equation of motion is

$$\frac{\mathrm{d}\boldsymbol{U}_\mathrm{p}}{\mathrm{d}t} = \boldsymbol{g} - \frac{\boldsymbol{U}_\mathrm{p} - \boldsymbol{U}}{\tau_\mathrm{p}}, \tag{20}$$

where $\mathrm{d}\boldsymbol{X}/\mathrm{d}t = \boldsymbol{U}_\mathrm{p}$,

$$\tau_\mathrm{p} = \frac{m_p}{3\pi\,\mu\,d\,(1 - f_\mathrm{c})}$$

is the Stokes time, $m_p = \rho_\mathrm{p}\,(\pi d^3/6)$ is the particle mass of the spherical form, d is the particle diameter, ρ_p is the particle material density, $\mu = \rho\,\nu$ is the dynamic viscosity, $f_\mathrm{c} = 0.15\mathrm{Re}_\mathrm{p}^{0.687}$, and $\mathrm{Re}_\mathrm{p} = |\boldsymbol{U}_\mathrm{p} - \boldsymbol{U}|d/\nu$ is the particle Reynolds number.[3] The key parameter of the problem is the Stokes number $\mathrm{St} = \tau_\mathrm{p}/\tau_\mathrm{k}$ which is based on the particle Stokes time and the Kolmogorov timescale $\tau_\mathrm{k} = \tau_\mathrm{f}/\sqrt{\mathrm{Re}}$, where $\tau_\mathrm{f} = 1/u_\mathrm{rms}k_\mathrm{f}$ is the turbulent integral timescale, $\mathrm{Re} = u_\mathrm{rms}/\nu k_\mathrm{f}$ is the fluid Reynolds number and u_rms is the root mean square fluid velocity. The parameter f_c is used for inertial particles with $\mathrm{Re}_\mathrm{p} \geq 1$. Even though f_c is indeed used for calculating the particle forces in the simulations it is set to zero when calculating the Stokes number of a given particle size. This is justified by the fact that for all particles considered here f_c is always very small and, furthermore, the Stokes number is only used for illustrative purposes. The ratio between the particle material density and the fluid mass density is $S = \rho_\mathrm{p}/\rho_0$, and for all simulations $S = 1000$ outside the cooled zone.

To demonstrate robustness of the effect of particle accumulation in the vicinity of mean temperature minimum we use three different models for the dynamic viscosity μ: (i) $\mu = \mu_*\sqrt{T(z)/T_0}$, where $\mu_* = \mathrm{const}$; (ii) μ=const; (iii) $\mu = \rho(z)\,\nu$, where $\nu = \mathrm{const}$.

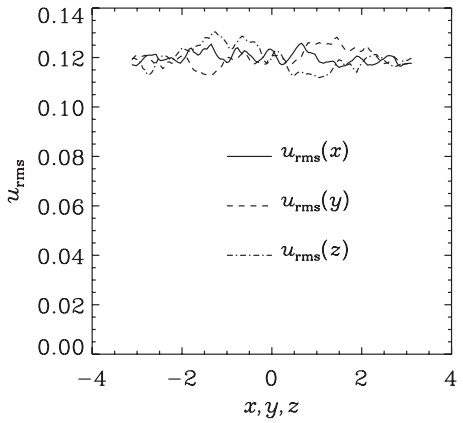

FIG. 3. The instantaneous *x*, *y*, and *z* profiles of u_rms for a simulation with forcing at $k_f = 5$ and $\mathrm{Re} = 240$.

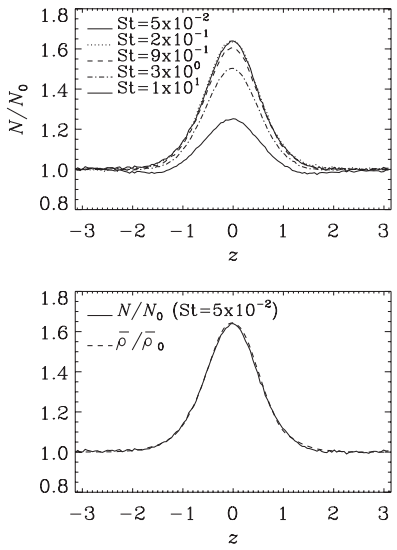

FIG. 4. Upper plot: vertical profile of the mean number density of inertial particles for different Stokes numbers for simulations with $k_f = 5k_1$, Re = 240 in the case where the kinematic viscosity is kept constant and no gravity. Here, the Stokes number St is based on the fluid density and temperature at the boundary. Lower plot: same as the upper plot, but showing the particle number density only for the smallest Stokes numbers together with the fluid mass density.

For most of the simulations the number of Eulerian grid points are 128^3, while the number of Lagrangian particles is 5×10^5. It has been verified that increasing the number of grid points up to 512^3 or the number of particles up to 10^7 has no effect on the results.

In simulations without gravity, periodic boundary conditions are used in all directions both for the fluid and for the particles. When gravity is taken into account in the simulations, particles are made elastically reflecting from the vertical boundaries. It has been checked that adding small Brownian diffusion of particles does not affect the results.

In all our simulations, gravity is ignored in Eq. (18) for the fluid, but for the simulations presented in Sec. III C it is included in Eq. (20) for particle motions. This situation has direct applications to atmospheric turbulence with lower troposphere temperature inversions, where the density scale height due to gravity is about 8 km, while the characteristic temperature inhomogeneity scale inside the temperature inversions is about 500–800 m, and the integral scale of turbulence is about 50–100 m (see Ref. 2).

C. Inertial particles in the absence of gravity

Let us first discuss the results of the numerical simulations concerning the formation of the inertial particle inhomogeneities in the absence of gravity. In Figs. 4 and 5 we plot the vertical profile of the mean number density of particles for simulations with $k_f = 5k_1$, Re = 240, different Stokes numbers, and different formulations for the dynamic viscosity. Inspection of these figures shows that, for a wide range of Stokes numbers, the maximum in the particle number density is located in the vicinity of the mean temperature minimum.

In the absence of gravity ($W_g = 0$), the parameter α is given by $\alpha = -\ln \tilde{N} / \ln \tilde{T}$; see Eq. (14) for $D_T \gg D$. In Fig. 6 the Stokes number dependence of the parameter α is shown for different Reynolds numbers and different forcing scales. It can be seen that the parameter α reaches its maximum value for $\mathrm{St}_* \approx 0.2$, while for Stokes numbers $\mathrm{St} > \mathrm{St}_*$, the value of α decreases monotonically. A critical Stokes number, St_c, separating the large and small Stokes number regimes might be defined such that $\alpha \geq 1$ for $\mathrm{St} < \mathrm{St}_c$, while for $\mathrm{St} > \mathrm{St}_c$ the parameter α is decreasing steeply with increasing Stokes number.

Since in the simulations the rms Mach number is not very small (around 0.2), the maximum value of the parameter α is only slightly larger than 1. Indeed, the contribution of particle inertia to the coefficient α for small Stokes numbers is determined by $\nabla \cdot \boldsymbol{U}_p \propto (\tau_p/\overline{\rho})\, \nabla^2 p$. On the other

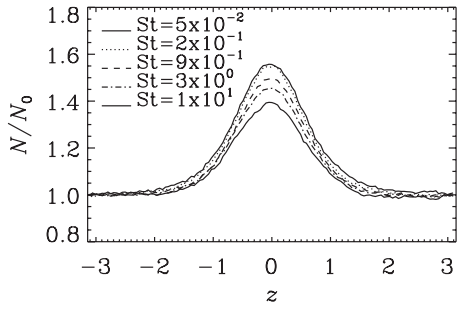

FIG. 5. The same as the upper plot of Fig. 4 but for the case where the dynamic viscosity is $\mu = \mu_* \sqrt{T(z)/T_0}$, μ_* is kept constant, and the Stokes number St is based on the fluid density and temperature at the boundary.

hand, $\nabla^2 p/\overline{\rho} \propto c_s^2 \nabla^2 \theta/\overline{T} \propto M^{-2} u_{\rm rms}^2 \nabla^2 \theta/\overline{T}$, where $M = u_{\rm rms}/c_s$ is the Mach number, and c_s is the speed of sound. The deviation of the parameter α from 1 is of the order of (see Ref. 36)

$$\alpha - 1 \propto \frac{\tau_p}{\tau_f} M^{-2}. \tag{21}$$

In this estimate we took into account that $|\overline{\boldsymbol{U}\,\nabla^2\theta}| \sim \ell^{-2} |\overline{\boldsymbol{U}\,\theta}|$ and the turbulent heat flux is $\overline{\boldsymbol{U}\,\theta} = -\kappa_T \nabla \overline{T}$, where $\kappa_T \sim \tau_f u_{\rm rms}^2$ and $\ell = \tau_f u_{\rm rms}$.

Therefore, decreasing the Mach number causes α to increase due to particle inertia. For instance, in atmospheric turbulence the Mach number is of the order of $(0.1 - 3) \times 10^{-3}$ and α is about 10 (see Ref. 37). On the other hand, the observed effect of accumulation of inertial particles occurs only for turbulent flows with large fluid Reynolds number. Decreasing the Mach number in the PENCIL CODE will either result in a shorter time step or a lower Reynolds number. This implies that we cannot easily reach at the same time small Mach numbers and large fluid Reynolds number. Therefore, the observations of the accumulation of inertial particles in the parameter range $\alpha \gg 1$ is not currently possible with the PENCIL CODE.

The parameter α for the heavy particles decreases strongly with $\tau_p \propto$ St (see Fig. 6 in the large Stokes number regime). Furthermore, it is expected that, in the large Stokes number regime, α is independent of Re for a particle as long as $u_{\rm rms}$ and k_f are kept constant. This is due to the fact that particles with $\tau_p \sim \tau_f$ are affected primarily by the largest turbulent eddies in the flow. This is because the smaller turbulent eddies have turnover times much shorter than the particle's Stokes time, and they cannot accelerate the particles. Since the Stokes number is based on the Kolmogorov time τ_k, this implies that $\mathrm{St}_c \propto \sqrt{\mathrm{Re}}$, which is indeed what is found in Fig. 6.

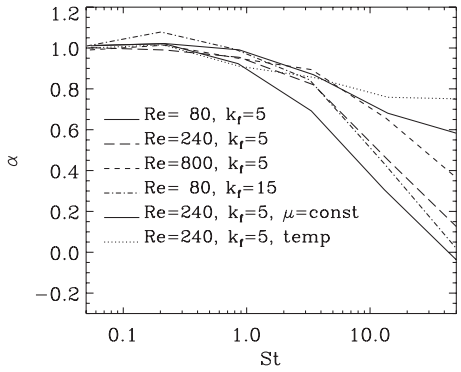

FIG. 6. The parameter α versus the Stokes number St for different Reynolds numbers and forcing wavenumbers in the absence of gravity. For the dashed-triple-dotted line the dynamic viscosity, μ, is kept constant while for the dotted line named "temp" the dynamic viscosity $\mu = \mu_* \sqrt{T(z)/T_0}$, where μ_* is kept constant. For all other lines the dynamic viscosity, $\mu = \rho(z)\nu$, where the kinematic viscosity ν is kept constant. Here, the Stokes number St is based on the values of fluid density and temperature at the boundary.

TABLE III. The coefficient α, the relative maximum of the particle number density and profile width for simulations with $k_f = 5k_1$, Re = 240 and for different formulations of the dynamic viscosity: (i) in the model f_1 the dynamic viscosity is $\mu = \mu_* \sqrt{T(z)/T_0}$, where μ_* is constant; (ii) in the model f_2 the dynamic viscosity is constant; (iii) in the model f_3 the dynamic viscosity $\mu = \rho(z)\,\nu$, where the kinematic viscosity ν is constant. The profile width L_N is given at the level when the number density is decreased in e times.

	α			N_{max}/N_0			Profile width		
St	f_1	f_2	f_3	f_1	f_2	f_3	f_1	f_2	f_3
0.1	1.00	1.01	1.00	1.55	1.66	1.63	0.88	0.80	0.79
1	0.91	0.98	0.95	1.49	1.62	1.60	0.86	0.80	0.79
10	0.80	0.75	0.59	1.42	1.44	1.35	0.90	0.82	0.81
14	0.76	0.68	0.45	1.39	1.39	1.25	0.90	0.83	0.82

When experiencing a high fluid density, a particle in the large Stokes number regime will more easily be accelerated by turbulence if the kinematic viscosity ν is constant than if the dynamic viscosity $\mu = \rho\nu$ is constant. This is due to the fact that for constant ν a high fluid density is associated with a smaller Stokes number, while for constant μ the Stokes number is independent of the fluid density. Due to this it is expected that particles with large Stokes numbers tend to be more depleted from the high density regions when ν is constant than when μ is constant. This explains why the simulation shown in Fig. 6 with constant μ has a much shallower fall-off with increasing Stokes number in the large Stokes number regime than the simulations with constant ν.

If the integral scale of turbulence is close to the scale of the thermal cooling layer, a particle trapped inside a turbulent eddy might travel across the whole cooling zone during one eddy turnover time. This will effectively smear out the peak of the particle number density, and consequently also decrease the parameter α. For simulations with $k_f = 5k_1$, the integral scale is comparable to the cooling scale, and the peak of α for $k_f = 5k_1$ is lower than for simulations with $k_f = 15k_1$ (see Fig. 6). This trend is expected to continue for yet larger k_f.

In addition, Fig. 6 shows that the difference in the parameter α determined for different formulations of the dynamic viscosity μ, is very small for $\mathrm{St} \ll 1$, and it is small for $\mathrm{St} \sim 1$. The real difference in the parameter α is only observed for large Stokes numbers, $\mathrm{St} > 10$ (see Table III). In this case, the largest value of α occurs for the dynamic viscosity $\mu = \mu_* \sqrt{T(z)/T_0}$, where $\mu_* = \text{const}$. On the other hand, the difference in relative maximum of the particle number density and the profile width for different formulations of dynamic viscosity is very minor (see Table III). Also scale-separation increases the effect of particle accumulation for $\mathrm{St} > 1$ [see Fig. 6]. However, using different parameters and different formulations of the dynamic viscosity, we always observe the effect of particle accumulation in the vicinity of the mean temperature minimum. This is an indication of the robustness of this phenomenon.

D. Inertial particles with gravity

For heavy inertial particles with large Stokes numbers, gravity plays a crucial role, and must be included in the simulations. In Fig. 7, the mean particle number density is shown as a function of vertical position z for simulations with $\mathrm{St} = 1$, $k_f = 5k_1$, and different gravitational accelerations.

In the following, gravity is measured in the units of $g_0 = D_T/(\tau_k L)$, so that $g/g_0 = \mathrm{St}^{-1}\, L/L_g$ for a particle of Stokes number unity. Here, $L_g = D_T/W_g$ is the characteristic scale of the mean particle number density variations due to the gravity for an isothermal case, $D_T = u_{rms}/3k_f$ is the turbulent diffusion coefficient, and L is the height of the box.

As the particle sedimentation velocity is increased, the particle number density profile is more and more tilted, as expected. For large particle sedimentation velocity ($g/g_0 = 200/3$), almost all particles have accumulated at the lower wall of the box (see Fig. 7).

In Fig. 8, the vertical profile of the particle number density is shown for $g/g_0 = 2/3$ and different Stokes numbers. By fitting these results with Eq. (14), the parameter α is found to be about 1 for the three smallest Stokes numbers in Fig. 8, while for $\mathrm{St} = 3.5$ and $\mathrm{St} = 14$ a

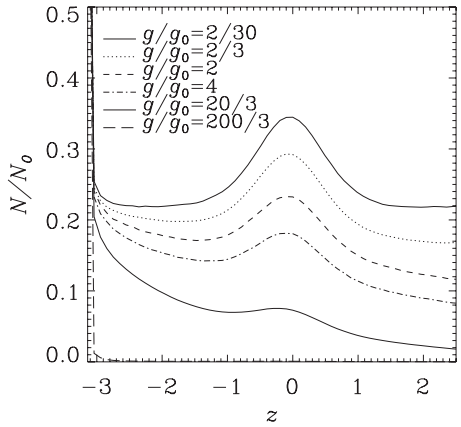

FIG. 7. Vertical profile of the mean number density for different gravitational accelerations, St = 1 and $k_f = 5k_1$, where the kinematic viscosity ν is kept constant.

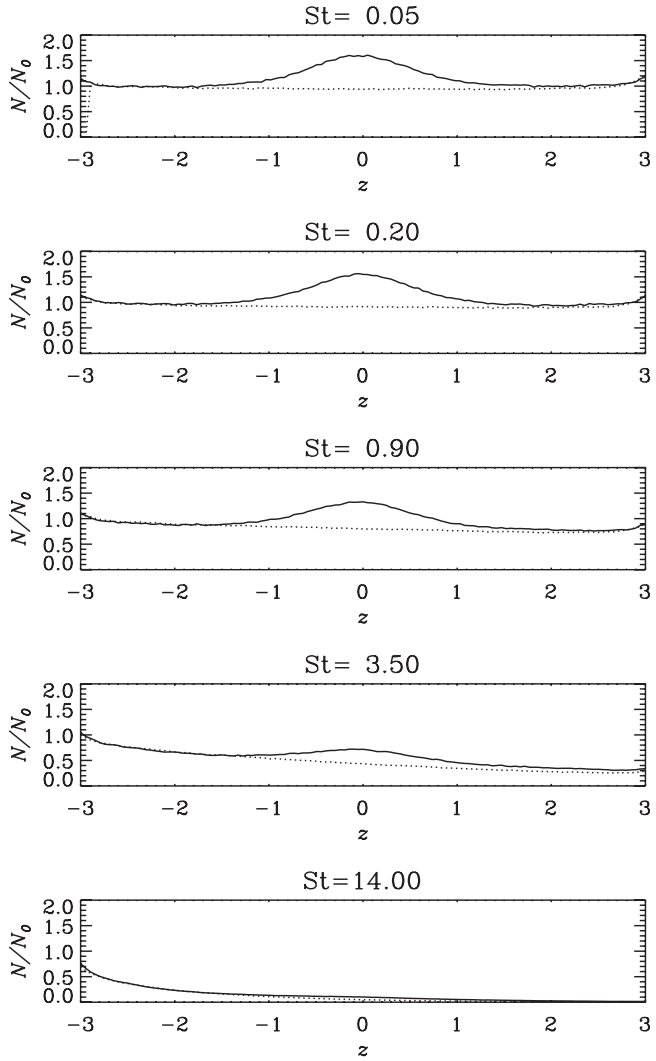

FIG. 8. Vertical profile of the mean number density (solid line) for $g/g_0 = 2/3$, $k_f = 5k_1$ and different Stokes numbers which are based on the fluid density and temperature at the boundary. Here, the kinematic viscosity ν is kept constant. The dotted line represent the isothermal reference case.

best fit of α is found around 0.8 and 0.5, respectively. For large Stokes numbers the maximum particle number density is found near the bottom wall of the box due to the large sedimentation velocity.

E. Non-inertial particles

For comparison with the numerical simulations performed for inertial particles in a Lagrangian framework, we describe in this section numerical simulations for non-inertial particles, where the equations for both, fluid and particles are solved by employing DNS in an Eulerian framework. In particular, we now solve Eq. (1) for the number density of non-inertial particles n_p with $\boldsymbol{U}_p = \boldsymbol{U}$, and the fluid density ρ, the fluid velocity $\boldsymbol{U}$, and the specific entropy s, using again the PENCIL CODE.[51] For these simulations the resolution is 128^3. For the fluid we apply the same conditions as was described in Subsections III A–III D. In particular, the periodic boundary conditions are used in these simulations in three directions for Eqs. (1) and (17)–(19).

Non-inertial particles are characterized by the following dimensionless parameters: $\mathrm{Pe} = u_{\mathrm{rms}}/Dk_{\mathrm{f}}$ is the Péclet number and $\mathrm{Sc} = \nu/D$ is the Schmidt number. The results of the simulations, shown in Fig. 9, demonstrate the accumulation of non-inertial particles in the vicinity of the maximum of the mean fluid density (or the minimum of the mean fluid temperature). This is in agreement with the theoretical predictions.[30,31]

The results shown in Fig. 9 demonstrate that the profiles of the mean fluid density and the mean particle number density are similar in numerical simulations with large Péclet and Reynolds numbers. However, when the Péclet number, $\mathrm{Pe} = \mathrm{Re}\,\mathrm{Sc}$ is not large, the molecular diffusion D becomes important, and the profiles of the mean fluid density and the mean particle number density are, according to Eq. (11), no longer similar.

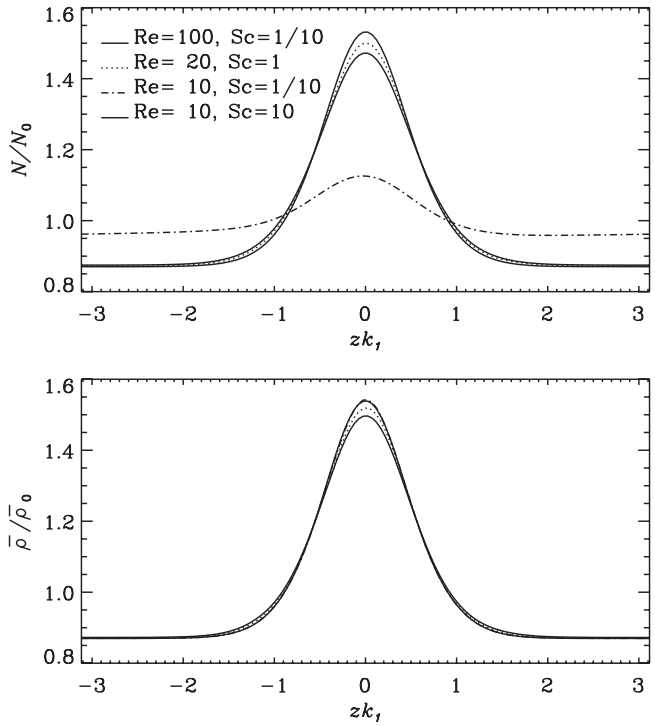

FIG. 9. Vertical profiles of the mean number density (upper panel) and the mean fluid density (lower panel) of non-inertial particles for simulations with $k_{\mathrm{f}} = 5k_1$ and different Reynolds and Schmidt numbers.

IV. DISCUSSION AND CONCLUSIONS

This study is the first numerical demonstration of the existence of the phenomenon of turbulent thermal diffusion of inertial and non-inertial particles in forced, temperature-stratified turbulence. The inertial particles are described using a Lagrangian framework, while non-inertial particles and the fluid flow are determined using an Eulerian framework. The phenomenon of turbulent thermal diffusion has been studied for different Stokes and fluid Reynolds numbers, Péclet numbers as well as different forcing scales of the turbulence. Furthermore, the effect of gravity has been included in the simulations.

We have demonstrated in the paper that even in stationary, homogeneous, but stratified turbulence there is accumulation of particles in the vicinity of the mean temperature minimum due to the turbulent thermal diffusion, rather than, e.g., the gravity effect. In particular, we have performed numerical simulations when the gravity effect was switched off (i.e., the terminal fall velocity of particles was zero). In this case we do observe the particle accumulation in the region with the mean temperature minimum.

Note that the minimum of the mean temperature in the numerical simulations was located at the center of the box. Therefore, above the mean temperature minimum the turbulence is stably stratified, while below it the turbulence is unstably stratified. In all simulations, with different parameters and different formulations of the dynamic viscosity, we always observe the effect of particle accumulation in the vicinity of the mean temperature minimum due to turbulent thermal diffusion for $\mathrm{St} < 1$. This implies that this effect is robust and has general validity, i.e., it should exist in different types of stratified turbulence. The results of the numerical simulations are in agreement with theoretical studies,[30,31,41,42] laboratory experiments[33,35,36] and atmospheric observations.[37] When $\mathrm{St} > 1$, this effect is decreasing with Stokes number.

The mean-field approach that describes the large-scale particle dynamics, implies that there is a separation of scales. In our simulations k_f/k_1 is varied from 5 to 15 (i.e., the integral scale of the turbulence is 5–15 times less than the size of the box). On the other hand, as follows from Figs. 4, 5, and 7–9, the typical scale of the inhomogeneity of particle number density is only 3 times smaller than the size of the box. This implies that the characteristic scale of the particle inhomogeneity formed due to the turbulent thermal diffusion is larger than the integral scale of the turbulence.

The theory of the phenomenon of turbulent thermal diffusion which is only developed for small Stokes numbers, does not allow for a detailed quantitative comparison when the Stokes numbers are not small. The quantitative comparison is possible only when the Stokes numbers are small (e.g., for transport of aerosols in atmospheric turbulence, the numerical simulations with non-inertial particles). For example, in Fig. 4 (low panel) we show the case of small Stokes number ($\mathrm{St} = 0.05$) when inertia of particles is negligible and particles can be considered as non-inertial. In this case for large Péclet numbers $D_\mathrm{T} \gg D$ and the steady-state solution of Eq. (8) is $N/N_0 = \overline{\rho}/\overline{\rho}_0$ (see Eq. (11)). This is just what is observed in the lower panel of Fig. 4, where the profiles of the normalized particle number density coincides with the profile of the fluid density. Note also that a comparison of turbulent thermal diffusion with other mechanisms in particle transport (namely, thermophoresis of particles, turbulent diffusion, and turbophoresis) shows that these effects in our simulations are smaller than turbulent thermal diffusion.

ACKNOWLEDGMENTS

This work was supported in part by the Norwegian Research Council project PAFFrx (186933) (NELH), by European Cooperation in Scientific and Technical Research (COST) Action MP0806, by the European Research Council under the Atmospheric Research Project No. 227915 and by a grant from the Government of the Russian Federation under Contract No. 11.G34.31.0048 (N.K., I.R.), and by the European Research Council under the AstroDyn Research Project 227952 (A.B.). The authors acknowledge the hospitality of NORDITA.

[1] G. T. Csanady, *Turbulent Diffusion in the Environment* (Reidel, Dordrecht, 1980).
[2] A. K. Blackadar, *Turbulence and Diffusion in the Atmosphere* (Springer, Berlin, 1997).
[3] C. T. Crowe, J. D. Schwarzkopf, M. Sommerfeld, and Y. Tsuji, *Multiphase Flows with Droplets and Particles*, 2nd ed. (CRC, New York, 2011).

[4] Z. Warhaft, "Passive scalars in turbulent flows," Annu. Rev. Fluid Mech. **32**, 203 (2000).
[5] Z. Warhaft, "Laboratory studies of droplets in turbulence: Towards understanding the formation of clouds," Fluid Dyn. Res. **41**, 011201 (2009).
[6] S. Balachandar and J. K. Eaton, "Turbulent Dispersed Multiphase Flow," Annu. Rev. Fluid Mech. **42**, 111 (2010).
[7] R. A. Shaw, "Particle-turbulence interactions in atmospheric clouds," Annu. Rev. Fluid Mech. **35**, 183 (2003).
[8] R. E. Britter and S. R. Hanna, "Flow and dispersion in urban areas," Annu. Rev. Fluid Mech. **35**, 469 (2003).
[9] A. Khain, M. Pinsky, T. Elperin, N. Kleeorin, I. Rogachevskii, and A. Kostinski, "Critical comments to results of investigations of drop collisions in turbulent clouds," Atmos. Res. **86**, 1 (2007).
[10] V. S. Safronov, *Evolution of the Protoplanetary Cloud and Formation of Earth and the Planets*, NASA Tech. Transl. F-677 (Israel Sci. Transl., Jerusalem, 1972).
[11] T. Takeuchi, *Small Bodies in Planetary Systems*, Lecture Notes in Physics Vol. 758 (Springer, Berlin, 2009), p. 1.
[12] L. S. Hodgson and A. Brandenburg, "Turbulence effects in planetesimal formation," Astron. Astrophys. **330**, 1169 (1998).
[13] A. Johansen, A. C. Andersen, and A. Brandenburg, "Simulations of dust-trapping vortices in protoplanetary discs," Astron. Astrophys. **417**, 361 (2004).
[14] A. Aliseda, A. Cartellier, F. Hainaux, and J. C. Lasheras, "Effect of preferential concentration on the settling velocity of heavy particles in homogeneous isotropic turbulence," J. Fluid Mech. **468**, 77 (2002).
[15] A. M. Wood, W. Hwang, and J. K. Eaton, "Preferential concentration of particles in homogeneous and isotropic turbulence," Int. J. Multiphase Flow **31**, 1220 (2005).
[16] J. Salazar, J. de Jong, L. Cao, S. Woodward, H. Meng, and L. Collins, "Experimental and numerical investigation of inertial particle clustering in isotropic turbulence," J. Fluid Mech. **600**, 245 (2008).
[17] H. Xu and E. Bodenschatz, "Motion of inertial particles with size larger than the Kolmogorov scale in turbulent flows," Physica D **237**, 2095 (2008).
[18] E. W. Saw, R. A. Shaw, S. Ayyalasomayajula, P. Y. Chuang, and A. Gylfason, "Inertial clustering of particles in high Reynolds-number turbulence," Phys. Rev. Lett. **100**, 214501 (2008).
[19] G. Boffetta, F. De Lillo, and A. Gamba, "Large scale inhomogeneity of inertial particles in turbulent flows," Phys. Fluids **16**, L20 (2003).
[20] J. Chun, D. L. Koch, S. L. Rani, A. Ahluwalia, and L. R. Collins, "Clustering of aerosol particles in isotropic turbulence," J. Fluid Mech. **536**, 219 (2005).
[21] L. Chen, S. Goto, and J. C. Vassilicos, "Turbulent clustering of stagnation points and inertial particles," J. Fluid Mech. **553**, 143 (2006).
[22] H. Yoshimoto and S. Goto, "Self-similar clustering of inertial particles in homogeneous turbulence," J. Fluid. Mech. **577**, 275 (2007).
[23] M. van Aartrijk and H. J. H. Clercx, "Preferential concentration of heavy particles in stably stratified turbulence," Phys. Rev. Lett. **100**, 254501 (2008).
[24] J. Bec, L. Biferale, M. Cencini, A. Lanotte, S. Musacchio, and F. Toschi, "Heavy particle concentration in turbulence at dissipative and inertial scales," Phys. Rev. Lett. **98**, 084502 (2007).
[25] J. Bec, L. Biferale, A. Lanotte, A. Scagliarini, and F. Toschi, "Turbulent pair dispersion of inertial particles," J. Fluid Mech. **645**, 497 (2010).
[26] P. A. Vaillancourt and M. K. Yau, "Review of particle–turbulence interactions and consequences for cloud physics," Bull. Am. Meteorol. Soc. **81**, 2851 (2000).
[27] H. Siebert, S. Gerashchenko, A. Gylfason, K. Lehmann, L. R. Collins, R. A. Shaw, and Z. Warhaft, "Towards understanding the role of turbulence on droplets in clouds: In situ and laboratory measurements," Atmos. Res. **97**, 426 (2010).
[28] A. Johansen and A. Youdin, "Protoplanetary disk turbulence driven by the streaming instability: nonlinear saturation and particle concentration," Astrophys. J. **662**, 627 (2007).
[29] A. Johansen, J. S. Oishi, M. M. Mac Low, H. Klahr, T. Henning, and A. Youdin, "Rapid planetesimal formation in turbulent circumstellar disks," Nature (London) **448**, 1022 (2007).
[30] T. Elperin, N. Kleeorin, and I. Rogachevskii, "Turbulent thermal diffusion of small inertial particles," Phys. Rev. Lett. **76**, 224 (1996).
[31] T. Elperin, N. Kleeorin, and I. Rogachevskii, "Turbulent barodiffusion, turbulent thermal diffusion and large-scale instability in gases," Phys. Rev. E **55**, 2713 (1997).
[32] A. Eidelman, T. Elperin, N. Kleeorin, A. Krein, I. Rogachevskii, J. Buchholz, and G. Grünefeld, "Turbulent thermal diffusion of aerosols in geophysics and in laboratory experiments," Nonlinear Processes Geophys. **11**, 343 (2004).
[33] J. Buchholz, A. Eidelman, T. Elperin, G. Grünefeld, N. Kleeorin, A. Krein, and I. Rogachevskii, "Experimental study of turbulent thermal diffusion in oscillating grids turbulence," Exp. Fluids **36**, 879 (2004).
[34] A. Eidelman, T. Elperin, N. Kleeorin, A. Markovich, and I. Rogachevskii, "Experimental detection of turbulent thermal diffusion of aerosols in non-isothermal flows," Nonlinear Processes Geophys. **13**, 109 (2006).
[35] A. Eidelman, T. Elperin, N. Kleeorin, I. Rogachevskii, and I. Sapir-Katiraie, "Turbulent thermal diffusion in a multi-fan turbulence generator with the imposed mean temperature gradient," Exp. Fluids **40**, 744 (2006).
[36] A. Eidelman, T. Elperin, N. Kleeorin, B. Melnik, and I. Rogachevskii, "Tangling clustering of inertial particles in stably stratified turbulence," Phys. Rev. E **81**, 056313 (2010).
[37] M. Sofiev, V. Sofieva, T. Elperin, N. Kleeorin, I. Rogachevskii, and S. S. Zilitinkevich, "Turbulent diffusion and turbulent thermal diffusion of aerosols in stratified atmospheric flows," J. Geophys. Res. **114**, D18209, doi:10.1029/2009JD011765 (2009).
[38] S. Chandrasekhar, "Stochastic problems in physics and astronomy," Rev. Mod. Phys. **15**, 1 (1943).
[39] A. I. Akhiezer and S. V. Peletminsky, *Methods of Statistical Physics* (Pergamon, Oxford, 1981).
[40] T. Elperin, N. Kleeorin, and I. Rogachevskii, "Formation of inhomogeneities in two-phase low-Mach-number compressible turbulent fluid flows," Int. J. Multiphase Flow **24**, 1163 (1998).

[41] T. Elperin, N. Kleeorin, I. Rogachevskii, and D. Sokoloff, "Passive scalar transport in a random flow with a finite renewal time: Mean-field equations," Phys. Rev. E **61**, 2617 (2000).
[42] T. Elperin, N. Kleeorin, I. Rogachevskii, and D. Sokoloff, "Mean-field theory for a passive scalar advected by a turbulent velocity field with a random renewal time," Phys. Rev. E **64**, 026304 (2001).
[43] R. V. R. Pandya and F. Mashayek, "Turbulent thermal diffusion and barodiffusion of passive scalar and dispersed phase of particles in turbulent flows," Phys. Rev. Lett. **88**, 044501 (2002).
[44] M. W. Reeks, "On model equations for particle dispersion in inhomogeneous turbulence," Int. J. Multiphase Flow **31**, 93 (2005).
[45] M. R. Maxey, "The gravitational settling of aerosol particles in homogeneous turbulence and random flow field," J. Fluid Mech. **174**, 441 (1987).
[46] A. S. Monin and A. M. Yaglom, *Statistical Fluid Mechanics* (MIT, Cambridge, 1975), Vol. 2.
[47] P. Chassaing, R. A. Antonia, F. Anselmet, L. Joly, and S. Sarkar *Variable density fluid turbulence* (Kluwer Academic, Dordrecht, 2002).
[48] S. K. Friedlander, *Smoke, Dust, and Haze. Fundamentals of Aerosol Dynamics* (Oxford University Press, New York, 2000).
[49] M. Caporaloni, F. Tampieri, F. Trombetti , and O. Vittori, "Transfer of particles in nonisotropic air turbulence," J. Atmos. Sci. **32**, 565 (1975).
[50] M. W. Reeks, "The transport of discrete particle in inhomogeneous turbulence," J. Aerosol Sci. **14**, 729 (1983).
[51] See http://pencil-code.googlecode.com for the Pencil Code, a high-order finite-difference code (sixth order in space and third order in time).
[52] N. E. L. Haugen and S. Kragset, "Particle impaction on a cylinder in a cross flow as function of Stokes and Reynolds numbers," J. Fluid Mech. **661**, 239 (2010).
[53] N. E. L. Haugen and A. Brandenburg, "Hydrodynamic and hydromagnetic energy spectra from large eddy simulations," Phys. Fluids **18**, 075106 (2006).
[54] W. Dobler, N. E. L. Haugen, T. A. Yousef, and A. Brandenburg, "Bottleneck effect in three-dimensional turbulence simulations," Phys. Rev. E **68**, 026304 (2003).